

19.4% -EFFICIENT LARGE AREA REAR-PASSIVATED SCREEN-PRINTED SILICON SOLAR CELLS

T. Dullweber^{*1}, S. Gatz¹, H. Hannebauer¹, T. Falcon², R. Hesse¹, J. Schmidt¹, and R. Brendel^{1,3}

¹*Institute for Solar Energy Research Hamelin (ISFH),
Am Ohrberg 1, D-31860 Emmerthal, Germany*

²*DEK Printing Machines Ltd, 11 Albany Road, Weymouth,
DT4 9TH, United Kingdom*

³*Department of Solar Energy, Institute of Solid-State Physics,
Leibniz Universität Hannover, Appelstrasse 2, D-30167 Hannover, Germany*

ABSTRACT: We have implemented a baseline solar cell process based on today's standard industrially manufactured silicon solar cells with conversion efficiencies up to 18.5% applying 125×125 mm² 2-3 Ωcm boron-doped Cz silicon wafers, screen-printed front and rear contacts, and a homogeneously doped 70 Ω/sq n⁺-emitter. Optimizing a print-on-print process, we reduce the silver finger width from 110 μm to 70 μm which increases the conversion efficiency up to 18.9% due to the reduced shadowing loss. In order to further increase the efficiency, we implement two different dielectric rear surface passivation stacks: (i) a silicon dioxide/silicon nitride stack and (ii) an aluminium oxide/silicon nitride stack. The rear contacts to the silicon base are formed by local laser ablation of the passivation stack and aluminium screen printing. The dielectric layer stacks at the rear decrease the surface recombination velocity from $S_{eff, rear} = 350$ cm/s for a full-area Al-BSF down to $S_{eff, rear} = 70$ cm/s and increase the internal reflectance from 61% up to 91%. The improved solar cell rear increases the conversion efficiency η up to an independently confirmed value of 19.4%. The detailed solar cell analysis reveals potential to further increase the conversion efficiency towards 20% in the near future.

Keywords: Silicon Solar Cell, Screen Printing, Rear Passivation

1 Introduction

About 80% of the world wide industrially manufactured silicon solar cells apply screen printing for the deposition of the silver front and aluminium rear metal contacts resulting in conversion efficiencies around 18% on monocrystalline silicon wafers [1]. Among others two loss mechanisms limit the conversion efficiency of these cells: (1) The silver (Ag) front side metallization with finger widths around 90 – 100 μm reflects about 7% of the incident solar radiation. (2) The screen-printed full-area aluminium (Al) back surface field (BSF) exhibits only a moderate passivation quality with typical rear surface recombination velocities (S_{rear}) ranging from 200 to 600 cm/s [2,3]. In addition, only about 70% of the infrared light reaching the aluminium rear contact is reflected back into the silicon wafer [4]. One promising approach to reduce the front side shading loss is the print-on-print (PoP) technique, where the silver front contact is deposited in two consecutive screen printing steps. Previous work on PoP demonstrated finger widths down to 75 μm [5] and aspect ratios up to 0.46 [5], resulting in an efficiency increase compared to single-printed cells by 0.2% [6,7]. The electrical and optical losses of the full-area Al-BSF at the rear side can be reduced by applying the PERC (passivated emitter and rear cell) solar cell design [8]. The following dielectric layers are most promising to be applied as rear passivation: thermally grown SiO₂ [9], plasma-enhanced chemical vapour deposited (PECVD) SiN_x [9], SiC_x [10] or SiO_x [11] and Al₂O₃ deposited by atomic layer deposition (ALD) [12] or PECVD [13]. The application of such dielectric layers to large area screen-printed PERC solar cells resulted in conversion efficiencies up to 19.6% [14-17]. Very recently, a conversion efficiency of 20.2% has been reported for the first time for screen printed PERC solar cells [18].

At the ISFH, we demonstrated conversion efficiencies of up to 19.0% and 19.4% [17] for large area screen printed PERC solar cells using Al₂O₃/SiN_x and SiO₂/SiN_x rear

passivation layer stacks, respectively. The cell front side was metalized applying a print-on-print process. In this paper, we present a detailed description of the processing sequence as well as an experimental analysis of the resulting solar cell parameters. An outlook is provided on further technological improvements showing the potential of conversion efficiencies exceeding 20%.

2 Standard screen-printed silicon solar cells

At ISFH, we have established a reference process for screen-printed silicon solar cells which we consider to be very close to today's standard industrial processing sequence. We use pseudo-square 125×125 mm² 2-3 Ωcm p-type boron-doped Cz-silicon wafers with a starting thickness of 200 μm. The process flow is shown in Fig. 1. After a cleaning procedure including a KOH-based damage etch, the wafers are textured on both sides in an alkaline KOH/IPA-based chemical bath. The n⁺-emitter is formed on both wafer surfaces by POCl₃ diffusion performed in a quartz-tube furnace, resulting in a sheet resistance R_{sheet} of 60 to 70 Ω/□. The phosphorus silicate glass (PSG) is removed by etching in HF. The front side is coated with a SiN_x antireflective layer with a refractive index of $n = 2.05$ and a thickness of about 70 nm. Afterwards, we screen print the Ag front contacts using a DEK PVP1200 printer and a commercially available Ag paste resulting in about 110 μm wide Ag fingers measured after firing as shown in Fig. 2 (b). The Al rear contact is full-area screen-printed applying a commercially available Al paste. Ag pads on the rear side are not printed since the focus of this study is on cell performance and no modules are fabricated. After the co-firing step in a conveyor belt furnace, a laser edge isolation is applied in order to reduce shunts.

The resulting standard screen-printed solar cells display conversion efficiencies η of up to 18.5% as shown in table 1, cell A. On a larger number of identically

processed standard screen printed solar cells, we determine the standard variation of the conversion efficiency to be $\pm 0.1\%$.

A: Standard	B: PoP	C: PERC
Wafer clean	Wafer clean	Wafer clean
		Rear protection layer
Texturing	Texturing	Texturing
Phos. diffusion	Phos. diffusion	Phos. diffusion
PSG etch	PSG etch	PSG + dielectric etch
		Rear Passivation
		Rear: PECVD SiN _x
PECVD SiN _x	PECVD SiN _x	PECVD SiN _x
		Rear: laser ablation
Ag screen printing	Ag screen printing	Ag screen printing
	Ag screen printing	Ag screen printing
Al screen printing	Al screen printing	Al screen printing
Co-firing	Co-firing	Co-firing
Edge isolation	Edge isolation	

Figure 1: Process flows of the different solar cells investigated in this paper. (A) Standard screen printed solar cell, (B) Print-on-print (PoP) screen printed cell, (C) passivated emitter and rear cell (PERC) with Al₂O₃/SiN_x, and with SiO₂/SiN_x rear passivation. Laser edge isolation is not required for the PERC cells due to the single-sided phosphorus diffusion.

Table 1: Solar cell (125 mm Cz wafer) parameters measured under standard testing conditions. Cell A refers to a standard screen-printed solar cell with a full-area Al-BSF and single-printed Ag front contacts. The cells B₁ and B₂ received a print-on-print Ag front side metallization with reduced finger width. Cell C applies a rear side passivation of Al₂O₃/SiN_x and cells D and E (156 mm Cz wafer) a SiO₂/SiN_x rear passivation, in addition to the PoP Ag metallization.

Cell	Type	η	V_{oc}	J_{sc}	FF
		[%]	[mV]	[mA/cm ²]	[%]
A	Ref.	18.5	633	37.0	79.2
B ₁	PoP	18.9	634	37.4	79.7
B ₂	PoP	18.7*	632	37.1	79.8
C	PERC	19.0*	652	38.9	75.1
D	PERC	19.4*	664	38.5	75.8
E	PERC	19.3	652	38.4	76.4

*independently confirmed by FhG-ISE CalLab

3 Print-on-print (PoP) silver front side metallization

The process flow of the PoP cells is identical to standard single-printed solar cells. However, the Ag front contact is deposited in two consecutive screen printing steps as indicated in column B of Fig. 1 using a DEK PVP1200 printer. Both screens used in the two printing steps are standard mesh type screens with a two bus bar/60 fingers layout. The number of fingers has been increased from 50 for single print to 60 for PoP in order to minimize resistive losses due to the significantly smaller finger

width. In the first Ag screen print step, we apply a commercially available Ag paste Ag1 which is designed to allow a good contact resistance to the emitter. The finger aperture of screen 1 is 50 μm . After drying at 200 $^{\circ}\text{C}$, the second Ag screen printing step follows using a commercially available Ag paste Ag2 with low specific resistivity in order to reduce the finger line resistance. The finger aperture of screen 2 is increased to 60 μm in order to avoid a contact during the second printing step between the emulsion of screen 2 and the Ag fingers of the first printing step. The second print is completed by a drying step at 200 $^{\circ}\text{C}$. Both printing steps are highly accurately aligned towards the four edges of the silicon wafer by a vision camera system in the PVP1200 printer which ensures $\pm 12.5 \mu\text{m}$ alignment accuracy at 6 sigma and hence an excellent alignment of the second print on the first print.

The resulting PoP Ag finger profile after firing is shown in the scanning electron microscope (SEM) cross section in Fig. 2 (a). For comparison a standard single printed Ag finger is displayed in Fig. 2 (b). The PoP process reduces the finger width from about 107 μm for single print down to 55 μm while maintaining a similar finger height of 21 μm . Since the line edge roughness of screen-printed fingers is relatively high, we additionally measure the average finger width by an optical light microscope and obtain values of $(70 \pm 5) \mu\text{m}$. Based on the screen layout parameters such as finger length and bus bar area, we estimate that the smaller finger width reduces the shadowing loss from 6.7% for single print down to 5.4% for print-on-print with 70 μm finger width.

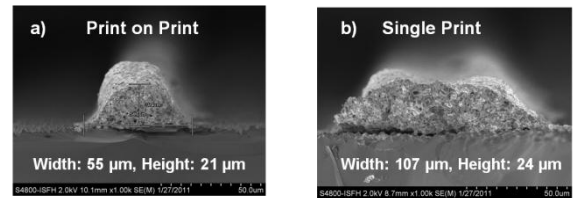


Figure 2: SEM cross section images of silver front contact fingers after firing on fully processed solar cells applying (a) print-on-print (PoP) screen printing with a finger width of 55 μm and (b) standard single printing with a finger width of 107 μm .

The measured cell parameters of the PoP solar cells B₁ and B₂ are shown in table 1. The PoP solar cells achieve conversion efficiencies of up to 18.9% which represents an improvement of 0.4% absolute compared to the standard single-printed solar cell A. The J_{sc} increase is explained by the reduced shadowing loss. In addition, the PoP cells show an excellent FF of up to 79.8% which indicates that there are no issues with respect to the line resistance or contact resistance. Besides increasing the conversion efficiency, due to the reduced finger width PoP also reduces the amount of Ag paste deposited on a solar cell by approximately 20 – 25%. This is important since the costs of the Ag paste significantly add to the total solar cell processing costs.

4 Passivated emitter and rear (PERC) screen-printed solar cells

Based on the process flow of the PoP screen-printed solar

cells, we have developed a process sequence which includes a passivation of the cell rear side applying dielectric layer stacks based on $\text{Al}_2\text{O}_3/\text{SiN}_x$ and $\text{SiO}_2/\text{SiN}_x$, as shown in the process flows of Fig. 1, column C. Before texturing and phosphorus diffusion, we deposit a dielectric protection layer on the rear side of the solar cell. The dielectric layer acts as a barrier against the alkaline texturing process as well as the phosphorus diffusion. Accordingly, only the front side of the solar cell is textured and phosphorus doped with a sheet resistance of about $70 \Omega/\square$ whereas the rear side remains planar and boron doped. The PSG etch after the diffusion step is slightly adjusted in order to remove the dielectric layer at the rear in addition to the PSG at the front. For the Al_2O_3 -passivated PERC cells the wafers are coated with a 10 nm plasma-assisted ALD- Al_2O_3 layer using process parameters as described in Ref. 19. For the SiO_2 passivated PERC cells we apply a dry thermal oxidation resulting in a 10 nm thick SiO_2 layer on the rear wafer surface and an approximately 25 nm thick SiO_2 layer on the front surface. Schematic drawings of the two PERC cells C and D are shown in Fig. 3 (a) and (b), respectively.

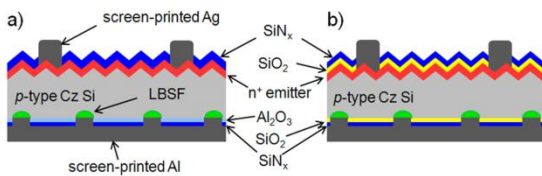


Figure 3: Schematic drawing of the PERC solar cells with screen-printed front and rear contacts with (a) $\text{Al}_2\text{O}_3/\text{SiN}_x$ and with (b) $\text{SiO}_2/\text{SiN}_x$ rear passivation stacks.

As shown in Fig. 4, the oxidation step for the PERC cells with $\text{SiO}_2/\text{SiN}_x$ passivation stack decreases the phosphorus concentration at the surface from $2 \times 10^{20} \text{ cm}^{-3}$ to $8 \times 10^{19} \text{ cm}^{-3}$ since the phosphorus atoms diffuse into the Si bulk during the high-temperature oxidation step. The sheet resistance increase from $70 \Omega/\square$ to $80 \Omega/\square$ as measured by the 4 point probe method.

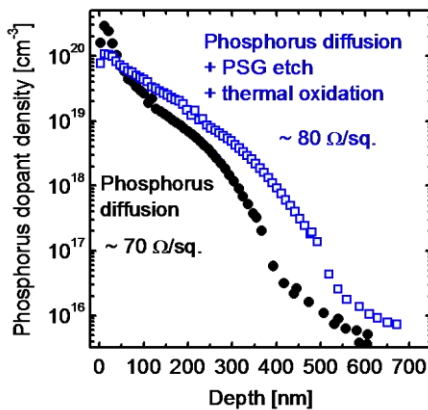


Figure 4: ECV doping profile measurements of phosphorus-diffused emitters of PERC cells with $\text{Al}_2\text{O}_3/\text{SiN}_x$ ($70 \Omega/\text{sq.}$) and with $\text{SiO}_2/\text{SiN}_x$ rear passivation stacks ($80 \Omega/\text{sq.}$).

Subsequently, the process flow continues identical for both rear passivation layers. We deposit a PECVD- SiN_x layer at the rear with a refractive index of $n = 2.05$ and a thickness of about 200 nm. The SiN_x layer at the rear meets several requirements: (1) it improves the surface recombination velocity after the firing process of the rear passivation layer for both, Al_2O_3 [19] as well as SiO_2 [20]. (2) It protects the 10 nm thin rear surface passivation layer from being etched by the Al paste during the firing process. (3) It improves the internal optical reflectance of the rear side since according to our investigations a dielectric layer thickness of at least 100 nm is required to obtain good reflection properties at the rear side. The front side is coated with a SiN_x antireflective layer of refractive index $n = 2.05$. The SiN_x thickness has been reduced for the SiO_2 -passivated PERC cell in order to compensate the about 25 nm thin SiO_2 at the front and achieve good antireflection properties. Afterwards, the dielectric passivation layer stacks at the rear side are locally ablated by laser contact opening (LCO) in order to form local line openings. The approximately $80 \mu\text{m}$ wide line openings are equidistantly spaced with a pitch between 1 mm and 2 mm. The width of the line contacts increases from $80 \mu\text{m}$ to approximately $140 \mu\text{m}$ during the firing process due to the chemical reaction of the Al paste with the silicon wafer and the passivation layer. We choose line openings instead of point contacts since line openings facilitate the formation of a deep and uniform local Al-BSF and hence reduce the surface recombination velocity compared to point contacts [21]. The Ag front contacts are deposited by the same PoP screen printing process as described in the previous section. However, for the rear-passivated cells the Ag finger width is around $90 \mu\text{m}$ instead of $70 \mu\text{m}$ for the PoP cells. The larger finger width for the PERC cells might partly be caused by the increased reflectivity of the rear side of the wafer which makes the wafer edge alignment of the PVP1200 screen printer less accurate. However, this is still subject to further analysis and optimization. First PoP evaluations on PERC cells applying a DEK Eclipse printer show very promising results. The Al rear contact is formed by standard full-area Al screen printing. We apply a different Al paste Al2 for the PERC cells as compared to paste Al1 used for the cells A and B in table 1. In reference 22 we show that the Paste Al2, which is designed for local Al contacts, achieves a deeper and more uniform local Al-BSF which results in a surface recombination velocity of 600 cm/s compared to 2000 cm/s for paste Al1. The firing process is comparable to the PoP cells B. The laser edge isolation is not required for PERC cells since only the front side is phosphorus doped.

The SEM cross section of the final PERC solar cell in Fig. 5 shows the local Al contact at the rear with a uniform Al-BSF above the Al-Si eutectic layer. The Ag finger is approximately $90 \mu\text{m}$ wide and the local Al contact has a width of approximately $140 \mu\text{m}$.

5 PERC solar cell analysis and discussion

Table 1 shows the measured cell parameters of the PERC solar cells C and D with $\text{Al}_2\text{O}_3/\text{SiN}_x$ and with $\text{SiO}_2/\text{SiN}_x$ rear passivation stacks on 125 mm Cz wafers. Cell E with $\text{SiO}_2/\text{SiN}_x$ rear passivation has been processed on 156 mm Cz wafers. The PERC cells are measured after

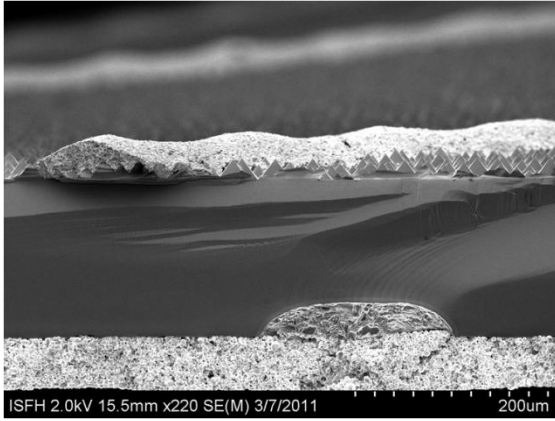


Figure 5: SEM cross section image of a screen-printed, rear-side-passivated PERC solar cell with local line contacts on the rear side. The cross section has been taken along the (110) crystallographic orientation with an angle of 45° with respect to the Ag fingers and local line contacts at the rear. Accordingly, horizontal dimensions of the finger width and the line contact width deduced from this image have to be divided by $\sqrt{2}$.

deactivation of boron-oxygen-related recombination by six hours simultaneously annealing at 140°C and illuminating with white light [23,24]. PERC solar cells C and D achieve independently confirmed conversion efficiencies of 19.0% and 19.4% compared to 18.9% for the full-area Al-BSF solar cell B₁. PERC cell E (156 mm wafer) shows an efficiency of 19.3%. All PERC solar cells show a strongly improved J_{sc} of up to 38.9 mA/cm^2 which is an increase of 1.5 mA/cm^2 compared to the full-area Al-BSF reference cell. Moreover, the $\text{SiO}_2/\text{SiN}_x$ -passivated PERC cell D shows a significantly improved open circuit voltage V_{oc} of 664 mV compared to the full-area Al-BSF cell with $V_{oc} = 634\text{ mV}$. However, the fill factor FF of the PERC solar cells up to 76.4% (cell E) are much lower compared to the FF of 79.8% for the reference cell B₂. The decreased FF is caused by an increased series resistance from $0.6\ \Omega\text{cm}^2$ for the full Al-BSF reference cells up to $1.3\ \Omega\text{cm}^2$ and $1.6\ \Omega\text{cm}^2$ for the PERC cells C and D, respectively. One contribution to the series resistance of the PERC solar cells is caused by the lateral current flow of the majority charge carriers in the silicon wafer to the local rear contacts. We calculate this additional series resistance contribution $R_{s,Lines}$ by applying the analytical model proposed by Plagwitz [25]:

$$R_{s,Lines} = \frac{\rho\rho}{2\pi} \ln \left(\frac{2 \left(\sqrt{\cosh \frac{\pi a}{4W} + 1} \right)}{\sqrt{\cosh \frac{\pi a}{4W} - 1}} \right) + \rho W \left(1 - \exp \left(-\frac{W}{p} \right) \right) \quad (1)$$

which applies if

$$\tanh \frac{\pi a}{4W} \leq \frac{1}{\sqrt{2}} \quad (2)$$

Assuming a specific resistivity of $\rho = 2.5\ \Omega\text{cm}$ and a thickness $W = 180\ \mu\text{m}$ of the silicon wafer material and a width $a = 140\ \mu\text{m}$ of the Al line contacts, equation 2 is fulfilled and equation 1 results in $R_{s,Lines} = 0.16\ \Omega\text{cm}^2$ and

$0.31\ \Omega\text{cm}^2$ for pitches $p = 1\text{ mm}$ and 2 mm , respectively. This does not fully explain the strong increase of the total series resistance of the PERC cells C and D of $0.7\ \Omega\text{cm}^2$ and $1.0\ \Omega\text{cm}^2$. Another contribution to the series resistance is an increased contact resistance of the Al rear contact since the contact area of the PERC cells is reduced to 7 - 14% of the contact area of the full-area Al-BSF solar cells. Recent investigations determine a specific contact resistance ρ_c of $55\text{ m}\Omega\text{cm}^2$ [26] for local screen printed Al contacts which results in contact resistances $R_c = \rho_c / f$ of $0.3 - 0.8\text{ m}\Omega\text{cm}^2$ depending on the metallization fraction f . Accordingly, the increased series resistance of the PERC cells compared to the full area Al-BSF reference cells shown in table 1 is explained by the sum of the bulk contribution $R_{s,Lines}$ and the Al contact resistance R_c .

For a detailed analysis PERC and Al-BSF solar cells are characterized by measuring their reflectance and internal quantum efficiency (IQE) shown in Fig. 6. In the long-wavelength region $\lambda > 900\text{ nm}$ the dielectric rear surface passivation strongly improves the reflectivity and the IQE. In table 2 the rear surface recombination velocity $S_{eff,rear}$ and the internal reflectance R_{rear} are shown, extracted from the data in the long-wavelength region using the software LASSIE [27] which combines the extended IQE evaluation by Basore [28] with the improved optical model developed by Brendel [29]. We obtain $S_{eff,rear} = (70 \pm 30)\text{ cm/s}$ for PERC cell C and $S_{eff,rear} = (80 \pm 30)\text{ cm/s}$ for PERC cell D. The full-area Al-BSF solar cell B₂ shows a $S_{eff,rear}$ of $(350 \pm 100)\text{ cm/s}$. We calculate the expected $S_{eff,rear}$ by applying the analytical model proposed by Fischer [30]:

$$S_{eff,rear} = \left(\frac{R_{s,Lines} - \rho W}{\rho D} + \frac{1}{f S_{cont}} \right)^{-1} + \frac{S_{pass}}{1 - f} \quad (3)$$

The series resistance $R_{s,Lines}$ is described by equation 1 and the diffusion coefficient of the minority charge carriers is $D = 26.9\text{ cm}^2/\text{s}$. We assume a surface recombination velocity for the local Al-BSF of $S_{cont} = 600\text{ cm/s}$ [21]. On test wafers, we measure a surface recombination velocity for the rear-passivated area $S_{pass} = 5\text{ cm/s}$ for $\text{Al}_2\text{O}_3/\text{SiN}_x$ and $S_{pass} = 16\text{ cm/s}$ for $\text{SiO}_2/\text{SiN}_x$. Applying equation 3, we obtain $S_{eff,rear} = 79\text{ cm/s}$ for $\text{Al}_2\text{O}_3/\text{SiN}_x$ with a metallization fraction $f = a/p = 0.14$ ($p = 1\text{ mm}$) and $S_{eff,rear} = 53\text{ cm/s}$ for $\text{SiO}_2/\text{SiN}_x$ with $f = 0.07$ ($p = 2\text{ mm}$). The calculated $S_{eff,rear} = 79\text{ cm/s}$ is in excellent agreement with the measured value of cell C with $S_{eff,rear} = (70 \pm 30)\text{ cm/s}$ in table 2. The measured $S_{eff,rear} = (80 \pm 30)\text{ cm/s}$ of cell D slightly exceeds the calculated $S_{eff,rear} = 53\text{ cm/s}$ within the measurement error.

The $\text{Al}_2\text{O}_3/\text{SiN}_x$ -passivated PERC cell C has a similar emitter doping profile and SiN_x surface passivation as the full-area Al-BSF cell B₂. The IQE of cell C for $\lambda < 500\text{ nm}$ in Fig. 6 is slightly higher compared to cell B₂ due to a little higher emitter sheet resistance. The PERC solar cell D with $\text{SiO}_2/\text{SiN}_x$ rear and front passivation shows a higher reflectance in the short wavelength reflectance due to the difference in the front side antireflection coating. The IQE of cell D in the short wavelength region is

increased because of the significantly lower phosphorus concentration at the surface as shown in Fig. 4 which reduces the charge carrier recombination in the emitter bulk and surface [31].

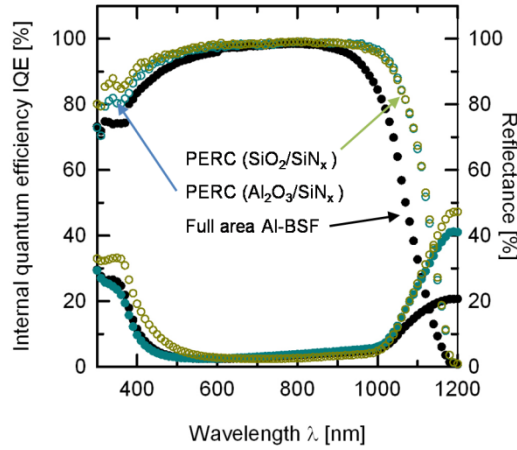


Figure 3: Comparison of internal quantum efficiency and reflectance between PERC solar cells with $\text{Al}_2\text{O}_3/\text{SiN}_x$ (cell C in table 1) and $\text{SiO}_2/\text{SiN}_x$ (cell D) passivation stacks at the rear and a full-area Al-BSF reference cell (B_2).

The reduced rear surface recombination velocity mostly explains the improvement in V_{oc} from 632 mV for cell B_2 to 652 mV for cell C as verified by PC1D simulations which predict a V_{oc} increase of 15 mV. The additional improvement in V_{oc} up to 664 mV for cell D is attributed to the optimized emitter doping profile shown in Fig. 4. The increase in J_{sc} of up to 1.5 mA/cm^2 for the PERC cells compared to a full-area BSF reference cell is due to the excellent rear surface passivation combined with an improvement of the internal rear reflectance from 61 % to 89 % and 91 %, respectively.

Table 2: Rear surface recombination velocity $S_{eff,rear}$ and internal reflectance R_{rear} of the PoP cell B_2 and the PERC cells C and D derived from the reflectance and IQE measurements shown in Fig. 6.

Cell	Rear side	Pitch [mm]	$S_{eff,rear}$ [cm/s]	R_{rear} [%]
B_2	Al-BSF	-	350 ± 100	61
C	$\text{Al}_2\text{O}_3/\text{SiN}_x$	1	70 ± 30	89
D	$\text{SiO}_2/\text{SiN}_x$	2	80 ± 30	91

6 Conclusions

Based on a solar cell process which is very similar to today's industrially manufactured standard screen-printed solar cells with conversion efficiencies up to 18.5%, we have shown that the print-on-print silver front side metallization reduces the finger width down to 70 μm and minimizes the shadowing loss to 5.4% which increases the conversion efficiency up to 18.9%. The implementation of a dielectric rear side passivation reduces the rear surface recombination velocity to $S_{eff,rear} = (70 \pm 30)$ cm/s for $\text{Al}_2\text{O}_3/\text{SiN}_x$ and $S_{eff,rear} = (80 \pm 30)$ cm/s for $\text{SiO}_2/\text{SiN}_x$ determined by IQE measurements.

The measured values are in good agreement with the calculated $S_{eff,rear}$ values applying an analytical model. Additionally, the dielectric layers strongly increase the internal reflectance up to 91% which results in independently confirmed conversion efficiencies up to 19.4% for large area silicon solar cells metallized by screen printing. The conversion efficiency is limited by a relatively low fill factor of 75.8% due to a high series resistance of the PERC cells which is mainly caused by a high specific contact resistance of 55 $\text{m}\Omega\text{cm}^2$ of the local Al contacts. Future improvements of the specific contact resistance should enable conversion efficiencies close to 20%. The Ag front side fingers deposited by print-on-print are 90 μm wide on the PERC cells instead of 70 μm for full-area Al-BSF reference cells. However, we expect that a further reduction of the finger width down to 70 μm for PERC cells is feasible by optimizing the screen printing process which should increase the efficiency by about 0.2%. The implementation of a selective emitter into the PERC cells represents another opportunity for further increasing the conversion efficiency by at least 0.3%. Accordingly, the results presented in this paper show the potential of large area screen-printed solar cells to achieve conversion efficiencies exceeding 20%.

Acknowledgements

We thank A. Lohse, B. Beier, T. Neubert, and F. Werner for their support in processing the solar cells as well as Heraeus und Ferro for providing the Ag and Al screen printing pastes. Parts of this work were funded by the German Federal Ministry for the Environment, Nature Conservation and Nuclear Safety under Contracts No. 0327529A and 0325296.

References

- [1] International Technology Roadmap for Photovoltaic (ITRPV.net), Results 2010, http://www.itrpv.net/doc/roadmap_itrpv_2011_brochure_web.pdf, March 2011, p. 15
- [2] S. Narasimha, A. Rohatgi, Proceedings 26th IEEE Photovoltaic Specialists Conference, (1997) 63
- [3] S. Peters, PhD thesis, University of Konstanz, (2004) 62
- [4] A. Lorenz et al., Proceedings 25th European Photovoltaic Solar Energy Conference, (2010) 2059
- [5] M. Galiazzo et al., Proceedings 25th European Photovoltaic Solar Energy Conference, (2010) 2338
- [6] T. Pham et al., Proceedings of the 25th European Photovoltaic Solar Energy Conference, (2010) 2378
- [7] T. Falcon, Proceedings 25th European Photovoltaic Solar Energy Conference, (2010) 1651
- [8] A. W. Blakers et al., Applied Physics Letters 55 (1989) 1363
- [9] J. Schmidt et al., Semicond. Sci. Technol. 16 (2001) 164
- [10] I. Martín et al., Applied Physics Letters 79 (2001) 2199
- [11] M. Hoffmann et al., Proceedings 22nd European Photovoltaic Solar Energy Conference, (2007) 1030
- [12] J. Schmidt et al., Progress in Photovoltaics 16 (2008) 461
- [13] H.-P. Sperlich et al., Proceedings 25th European Photovoltaic Solar Energy Conference, (2010) 1352
- [14] K. A. Münzer et al., Proceedings 25th European

- Photovoltaic Solar Energy Conference, (2010) 2314
- [15] T. Bösccke et al., Proceedings of the 37th IEEE Photovoltaic Specialists Conference, (2011) in press
- [16] J.-H. Lai et al., Proceedings of the 37th IEEE Photovoltaic Specialists Conference, (2011) in press
- [17] S. Gatz et al., Phys. Status Solidi RRL 5 (2011) 147
- [18] Schott Solar AG press release August 2011, <http://www.ffpress.net/Kunde/SOL/>
- [19] J. Schmidt et al., Phys. Status Solidi RRL 3 (2009) 287
- [20] T. Lauinger et al., Proceedings 13th European Photovoltaic Solar Energy Conference, (1995) 1291
- [21] J. Müller et al., Proceedings of the 1st SiliconPV Conference, (2011) in press
- [22] S. Gatz et al., Proceedings of the 1st SiliconPV Conference, (2011) in press
- [23] A. Herguth et al., Proceedings 21st European Photovoltaic Solar Energy Conference, (2006) 530
- [24] B. Lim et al., Phys. Status Solidi RRL 2 (2008) 93
- [25] H. Plagwitz, PhD thesis, University of Hannover, (2007)
- [26] S. Gatz et al., Proceedings 37th IEEE Photovoltaic Specialists Conference, (2011) in press
- [27] www.pv-tools.de
- [28] P. A. Basore, Proceedings 23rd IEEE Photovoltaic Specialists Conference, (1993) 147
- [29] R. Brendel, Thin-Film Crystalline Silicon Solar Cells, Wiley-VCH: Weinheim, (2003) 73
- [30] B. Fischer, PhD thesis, University of Konstanz, (2003)
- [31] M. J. Kerr et al., J. Appl. Phys. 89 (2001) 3821